

Rotating channel flow: Control and upstream currents

J. A. Whitehead & John Salzig

To cite this article: J. A. Whitehead & John Salzig (2001) Rotating channel flow: Control and upstream currents, *Geophysical & Astrophysical Fluid Dynamics*, 95:3-4, 185-226, DOI: [10.1080/03091920108203725](https://doi.org/10.1080/03091920108203725)

To link to this article: <https://doi.org/10.1080/03091920108203725>



Published online: 19 Aug 2006.



Submit your article to this journal [↗](#)



Article views: 55



View related articles [↗](#)



Citing articles: 2 View citing articles [↗](#)

ROTATING CHANNEL FLOW: CONTROL AND UPSTREAM CURRENTS

J.A. WHITEHEAD* and JOHN SALZIG

*Department of Physical Oceanography, MS #21, Woods Hole
Oceanographic Institution, Woods Hole MA 02543, USA*

(Received 16 November 2000; In final form 20 June 2001)

Theory and experiments are presented for critically controlled flow of a layer of inviscid rotating fluid. Flow is controlled by a level passage. For a wide upstream channel of fixed depth (i.e. constant potential vorticity) the volume flux on the right-hand wall is unaffected by passage flow. This suggests that specifying Bernoulli potential on the right-hand passage wall produces a physically well-posed condition. The specification results in one less dimensionless number than was required by previous formulations to specify flow in the controlled passage. The upstream flow needs the same number as before, so that a range of upstream conditions produce exactly the same passage flow. A laboratory study is conducted using a thin layer of water under air. This is pumped in steadily at various locations in a deep rotating upstream basin, with fluid leaving through a level passage. All currents in the upstream basin cross to the left-hand wall as the current approaches the passage over a sloping bottom. The current crosses back to the right-hand wall within the passage. Velocity profiles of currents agree reasonably well with constant potential vorticity theory. To the right of the detached upstream current is a closed gyre that connects the upstream flows (that have different patterns depending on source location) with the unique passage flows. The results suggest that gyres upstream of critically controlling passages in the ocean might serve as adjustment regions between the relatively unconstrained upstream flows and the tightly controlled passage flows.

Keywords: Rotating flow; Hydraulic control; Currents; Turntable experiments

1. INTRODUCTION

The subject of “rotating hydraulics” has come to mean the study of

*Corresponding author. E-mail: jwhitehead@whoi.edu
Current address: P.O. Box 1158, Ellsworth, ME 04605, USA.

stratified inviscid flows of a rotating fluid in which the flow is critically controlled by a passage. The simplest way to visualize critical control is to picture water pouring out of a pitcher. The lip of the pitcher is tipped below the free water surface in the container. At the lip, the flow adopts a flow speed equal to wave speed. In the pitcher itself, water speed is less than wave speed. In the water leaving the lip, speed exceeds wave speed. The trans-critical region transmits information about the lip configuration to the upstream water. This region also has a maximum possible volume flux leaving the region. Numerous books on hydraulics show that other internal properties are extremalized at the lip too. Rotation effects do not change the picture appreciably.

Probably the simplest possible configuration to understand ocean applications has inviscid rotating fluid with a free surface flowing out of a narrow passage from a big upstream reservoir. The flow in the passage is critically controlled by the configuration of the passage. Theoretical models include flows through gaps (Stern, 1974; Whitehead *et al.*, 1974; Gill, 1977; Shen, 1982; Nof and Olson, 1983; Pratt, 1983, 1984; Pratt and Armi, 1987), and gravity currents (Stern, 1980; Stern *et al.*, 1982; Griffiths and Hopfinger, 1983). Other configurations include shelf flows (Hughes, 1986a,b; 1987), coastal currents (Nof and Olson, 1983; Nof, 1988), planetary zonal currents (Armi, 1989; Woods, 1993; Haynes *et al.*, 1993; Johnson and Clarke, 2001), hydraulic jumps (Nof, 1986; Pratt, 1987), currents encountering obstacles such as the coast (Whitehead, 1985), bottom topography, (Borenas and Lundberg, 1986; Spitz and Nof, 1991; Nof, 1995), crossing the equator (Nof, 1990); and bounds on the above (Killworth, 1992; Killworth and McDonald, 1993; Killworth, 1994). Studies including the effect of friction include two layer exchange flow (Johnson and Ohlsen, 1994) and the effect of friction on a controlled flow without rotation (Pratt, 1986). Recently some questions about the nature of upstream currents have been analyzed (Pratt, 1997a,b, Pratt and Chechelnitzsky, 1997; Borenas and Whitehead, 1998).

Formulating such problems with a rotating fluid usually requires potential vorticity conservation. The first formulation assumed zero potential vorticity (Whitehead *et al.*, 1974). This is convenient because only one upstream condition (the elevation of the upstream water surface above the floor of the passage) is required to calculate

volume flux. The more general formulation of constant potential vorticity followed soon thereafter (Gill, 1977). This requires three upstream conditions instead of one. They are the upstream fluid depth; some measure of the strength of upstream currents near the walls; and the elevation difference between the upstream floor and the passage floor. From this, volume flux out of an exit passage can be calculated. A maximum value of the flux exists, and it was shown that the maximum flux produces a stationary small wave in the passage. Therefore, maximum flux is equivalent to a critical condition with Froude number equal to one.

Gill chose as the second upstream parameter ψ_i , the ratio of the volume flux of two currents on the two upstream walls. This parameter is convenient algebraically. However, it is not clear how one would impose a value of ψ_i for the inviscid problem. For instance, no thought experiments show how such a ratio could be controlled and held fixed for an inviscid fluid, since volume flux out of the passage is a component of the two currents. The dynamics of the upstream currents themselves can be analyzed if more physical processes are included. For instance, Pratt (1997a,b) and Pratt and Chechelnitsky (1997) developed conditions that include the effects of friction in the upstream basin.

Our primary motivation for asking about upstream conditions lies in the application to the ocean. There seems to be no way to pick a value for ψ_i in the ocean without already knowing the magnitude of the two flows approaching the gap. If these are known, their difference gives the value of flow out of the passage. Attempts have been made to estimate parameters near ocean gaps by using data from upstream regions (Whitehead, 1989, 1998). Using only bathymetric data and CTD information upstream of a number of deep ocean sills, it is possible to estimate volume flux through such gaps. There are a number of such estimates with "good" agreement (tens of percent) with direct measurements and some with "poorer" agreement (factors up to three). The question naturally arises about the nature of upstream conditions, particularly the currents supplying such flows. At present very little is known. The Denmark Strait overflow, for example, is abundantly measured downstream of the sill (Dickson *et al.*, 1990; Dickson and Brown, 1994). There are also recent measurements of currents at the sill region (Girton and Sanford, 1999; Girton, *et al.*, 2001). But upstream of the sill, there is only sparse information.

Density distribution is not resolved well enough to indicate if any localized currents exist. In addition, there are almost no direct current measurements upstream of the sill at all. Thus there is no direct information available to pick ψ_i . The same situation exists for the flow through the Vema Channel (Hogg *et al.*, 1982; Speer and Zenk, 1993); the Hunter Channel (Hogg *et al.*, 1999); the Faroe Bank Channel (Borenas and Lundberg, 1988; Saunders, 1990); Discovery Gap (Saunders, 1987); Charlie-Gibbs Fracture zone (Saunders, 1994); and the Samoa passage (Rudnick, 1997). The flow of Antarctic Bottom Water over the Ceara Abyssal Plain is resolved in an east-west channel centered roughly on the equator that serves as an entrance region (Hall *et al.*, 1997), and is more poorly resolved at about 4°N, (Whitehead and Worthington, 1982) but the control point location is unknown. In all such cases it would be extremely useful to know whether an upstream current might be expected along either the right-hand boundary facing the gap from upstream, the left-hand boundary, or both. It would also be very useful to know what the implications of upstream currents are on our present flux estimates.

Section 2 presents a physical argument and theory that indicates that information about the strength of any current flowing along the right-hand wall facing the passage from upstream is vital. (We take the convention that rotation is counterclockwise as in the Northern Hemisphere). In Section 3, flows resulting from the imposition of a source of currents in an upstream channel are examined in laboratory experiments. Comparison with theory has a velocity profile in good agreement with constant potential vorticity theory for the main current traversing the passage. A gyre is found upstream of the passage that seems to play an important role in coupling the upstream flow to the flow in the passage. Sections 4 and 5 discuss and then summarize the main results.

2. THEORY

A constant potential vorticity current can be pictured as arising from a channel of stagnant fluid with constant depth. The following thought experiment indicates that the value of volume flux imposed at the

right-hand wall of the upstream channel is a fixed variable that can be used to determine the flow out of a controlling passage. Let an upstream semi-infinite channel of counterclockwise rotating fluid of depth H be initially at rest with respect to the rotating fluid (Fig. 1). A gate is opened in a passage that allows removal of fluid from the channel. This sets up a critically controlled current in the channel in the same way that tilting a pitcher starts fluid pouring out. The onset of the current is accompanied by a Kelvin wave that propagates from the passage into the upstream portions of the channel along the left-hand wall. This wave produces a jump in the Bernoulli function and sets up a current (Gill, 1976) (For consistency, all further references to right and left-handed walls refer to the frame looking from the upstream channel to the passage as in Fig. 1). We assume that the channel is infinite in the upstream direction so the Kelvin wave and the upstream current it produces extend indefinitely in the upstream channel. For purposes of the thought experiment, let

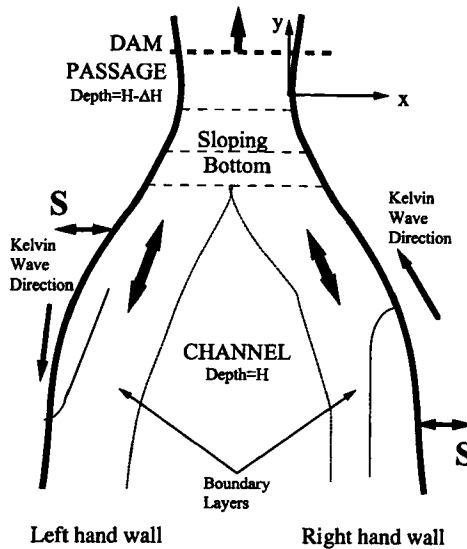


FIGURE 1 Sketch of the problem and definition of the coordinates. A passage of constant depth lies next to a semi-infinite flat bottom channel filled with fluid of depth H . After a gate is removed at a passage, a boundary layer establishes a current along the left-hand wall. Additional sources and sinks produce more currents along the walls, but only those on the right-hand wall reach the passage due to Kelvin wave propagation as shown.

the upstream channel be wider than the upstream Rossby radius of deformation. In this case the Kelvin wave occupies a boundary layer of Rossby radius width on the left-hand wall of the channel and does not alter the depth of the interior stagnant fluid in the upstream channel. No current along the right-hand upstream wall is produced by this Kelvin wave.

Next, imagine that additional currents are started by initiating pumps located in the walls of the channel labeled "S" in Fig. 1. These can be either sources or sinks as sketched. The following argument is based on the solutions of the characteristic equations by Pratt (1983, 1984). Because the ambient upstream currents are subcritical (i.e., less than the wave speed), the information about the newly formed current propagates away from the source along the wall in a normal direction to the right of a vector projecting tangentially from the wall into the channel. Currents that are set up by sources or sinks on the left-hand side of the channel extend only upstream – away from the passage. They influence neither the depth of stagnant interior fluid in the channel nor the flow in the exit passage. They merely get lost in the indefinitely large upstream region of the channel. This suggests that, in contrast to Gill's formulation which sets a value of fixed and constant ψ_i in the upstream basin, that the currents produced by sources or sinks on the left-hand wall do not alter the flow at the passage that has already been established. We conclude that *information about currents on the left-hand wall is not required to calculate flux out of the passage.*

In contrast, sources or sinks lying along the right-hand wall produce currents that extend downstream – toward the passage. These currents thereby could influence the flow through the passage. Since the opening of the gate and the ensuing change of current intensity in the passage produce Kelvin waves that propagate along the right-hand wall looking away from the passage, there is no change in the value of the flux along the right-hand wall looking toward the passage. This suggests that *only information about the right-hand wall currents is necessary to calculate flux out of the passage. In addition, currents along the right-hand wall are independent of the magnitude of flux out of the passage so that their values are not altered by the value of flux of the passage flow.* A thought experiment with sources or sinks turned on before opening the passage gives the same conclusion.

This information is to be incorporated in a formulation. The simplest such formulation assumes constant potential vorticity flow and is used here. The velocity distribution and fluid depth distribution across a constant potential vorticity current obey geostrophy and conservation of potential vorticity.

$$fv = g \frac{dh}{dx}, \quad \frac{1}{h} \left(\frac{dv}{dx} + f \right) = \frac{f}{H}. \quad (2.1a,b)$$

The coordinates are shown in Fig. 1 where v is velocity in the y direction. The coordinate at right angles to the direction of flow is x . The fluid depths are given by $h(x)$, which is height of the fluid above the local, level bottom and H , which is the depth of the fluid above the level bottom in a wide channel where the water is stagnant and at rest, (sometimes called the potential vorticity depth). The dynamic parameters are f , which is the Coriolis parameter, and g which is the acceleration due to gravity (and we could consider this to be reduced gravity $g' = g\Delta\rho/\rho$ if we are considering a layer of fluid of density $\rho + \Delta\rho$, lying below an infinitely deep region of stagnant fluid of density ρ). The well-known equation

$$\frac{d^2h}{dx^2} - \frac{f^2}{gH}h = -\frac{f^2}{g} \quad (2.2)$$

is found by combining (2.1a) and (2.1b). It has general solutions

$$h = H - A_{1i}e^{-x/R} - A_{2i}e^{x/R}, \quad v = \frac{g}{fR} (A_{1i}e^{-x/R} - A_{2i}e^{x/R}) \quad (2.3a,b)$$

where $R = \sqrt{gH}/f$. These equations are valid in both the upstream channel ($i=1$) and the passage ($i=2$). Without loss of generality we can consider the upstream channel being much wider than R . In that case there are boundary layers on both upstream sidewalls so that velocity far from the walls decays to zero. This is easily seen by redefining the constants in the relation for upstream depth h_u in the following way:

$$h_u = H - A'_{11}e^{(-x+x_1)/R} - A'_{21}e^{(x-x_r)/R}, \quad (2.4)$$

where x_i and x_r are locations of the upstream walls. In the upstream channel we will specify two things: the upstream stagnant fluid depth H , also specified by Gill (*loc. cit.*), and volume flux of the

upstream boundary current along the right-hand wall Q_{ur} . This flux is trapped on the right-hand side since (2.4) shows that for a very wide upstream channel ($x_r - x_l \gg R$) the velocity goes to zero away from the right-hand wall. In concert with the thought experiment, we presume the latter is due to volume flux sources or sinks of fluid with the interior value of potential vorticity on the right-hand upstream wall and is independent of the volume flux of the critically controlled flow at the passage. From (2.1a) the right-hand upstream volume flux is

$$Q_{ur} = \int_{-\infty}^0 v h_u dx = \frac{g}{2f} (h_{ur}^2 - H^2). \quad (2.5)$$

Thus the flux is related to h_{ur} , the fluid depth on the right-hand wall. The Bernoulli function

$$B = \frac{1}{2}v^2 + gh \quad (2.6)$$

is conserved along streamlines (Whitehead *et al.*, 1974) and it is convenient to determine it on the right-hand wall. This is because such a streamline will extend from an upstream point on the right-hand wall to the right-hand wall in the passage. Let us call the Bernoulli function $B = gH_r$ on the right-hand upstream wall. Then it is simple to show that

$$H_r = \frac{1}{2}H + \frac{1}{2}(h_{ur}^2/H). \quad (2.7)$$

This is a known quantity since H and Q_{ur} are known. This is in accord with the thought experiment that a pump along the right-hand upstream wall produces a Kelvin wave (and also a characteristic) that travels toward the passage. This signals that the pump is supplying or removing fluid. No information is required from flow along the left-hand wall to determine these constants. This agrees with the fact that a Kelvin wave moves from passage to upstream along the left-hand wall.

At the passage the bottom has shoaled by an amount ΔH . It is convenient to take the origin along the right-hand wall as sketched in Fig. 1. We define the depth of the fluid at the origin as h_0 and velocity as v_0 . Since the streamline along the right-hand upstream wall must

also be in contact with the right-hand wall in the passage, these two are related to the upstream Bernoulli function on the upstream right-hand wall by the Bernoulli equation that leads to

$$v_0 = \sqrt{2g(H_r - \Delta H - h_0)}. \quad (2.8)$$

This result generalizes an earlier study that had no current on the right-hand upstream wall and no bottom shoaling (Whitehead, 1989). Equations (2.3a,b) along the right-hand passage wall are

$$h_0 = H - A_{12} - A_{22}, \quad \sqrt{2g(H_r - \Delta H - h_0)} = \frac{g}{fR}(A_{12} - A_{22}) \quad (2.9a,b)$$

so that

$$A_{12}, A_{22} = \frac{1}{2} \left[H - h_0 \pm \sqrt{2H(H_r - \Delta H - h_0)} \right] \quad (2.10)$$

so equations (2.3a,b) are

$$\begin{aligned} h &= H - (H - h_0) \cosh(x/R) + \sqrt{2H(H_r - \Delta H - h_0)} \sinh(x/R), \\ v &= \frac{g}{fR} \left[-(H - h_0) \sinh(x/R) + \sqrt{2H(H_r - \Delta H - h_0)} \cosh(x/R) \right]. \end{aligned} \quad (2.11a,b)$$

Volume flux Q in the passage of width L is

$$\begin{aligned} Q &= \frac{g}{2f} [h_0^2 - (h(-L))^2] \\ &= \frac{g}{2f} \left(h_0^2 \left\{ H - \frac{1}{2} \left[H - h_0 + \sqrt{2H(H_r - \Delta H - h_0)} \right] e^{L/R} \right. \right. \\ &\quad \left. \left. - \frac{1}{2} \left[H - h_0 - \sqrt{2H(H_r - \Delta H - h_0)} \right] e^{-L/R} \right\}^2 \right), \\ &= \frac{gH^2}{2f} \left(\gamma^2 \left\{ 1 - \frac{1}{2} \left[1 - \gamma + \sqrt{2(1 - \delta - \gamma)} \right] e^{L/R} \right. \right. \\ &\quad \left. \left. - \frac{1}{2} \left[1 - \gamma - \sqrt{2(1 - \delta - \gamma)} \right] e^{-L/R} \right\}^2 \right) \end{aligned} \quad (2.12)$$

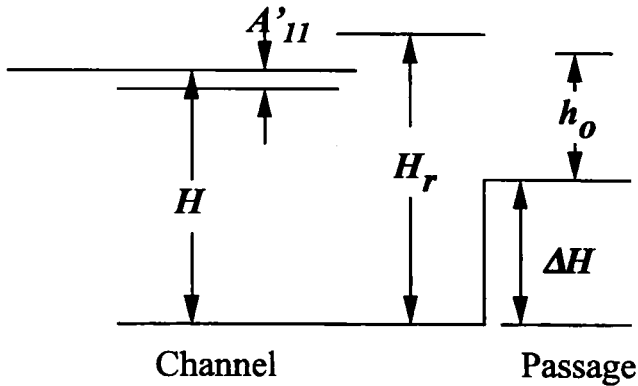


FIGURE 2 Heights along the right-hand wall at the passage and in the channel.

where $\gamma = h_0/H$, $\delta = (H + \Delta H - H_r)/H$. To help visualization of the definition of heights along the right-hand wall, they are sketched in Fig. 2. These heights determine the two governing dimensionless numbers γ and δ whose physical meaning is important to understand. The first is the ratio of fluid depth along the right-hand wall in the passage to the depth of stagnant fluid in the channel. Shear along the right-hand wall is positive, zero, or negative; and this depends respectively on whether γ is greater, equal to, or less than one. The maximum value is $\gamma = 1 - \delta$ for which velocity is zero at the right-hand wall of the passage. One can consider the parameter γ to be the free parameter that can be varied within a physically sensible range. As it varies, volume flux (if positive for any value of γ) passes through the maximum value that defines the critically controlled flux as discussed in the introduction. However, we will shortly adopt a substitute dimensionless number for γ .

The second dimensionless number expresses the difference between depth of interior channel fluid and depth of stagnant fluid (for which $\delta = 1 - \gamma$) at the right-hand wall of the passage, with both depths divided by depth of fluid in the channel. If δ is positive, fluid columns decrease in height between upstream and passage along the right-hand wall and vorticity is anticyclonic everywhere in the passage. However, if δ is negative and if fluid at the passage has the maximum possible value of γ , fluid columns stretch between upstream and passage along the right-hand wall and vorticity is cyclonic at the wall.

Let us compare equation (2.12) with Gill's Eq. (5.13) that relates a collection of dimensionless flow variables. In his notation the average scaled fluid depth is \bar{D} . This is related to the two geometric variables Δ and t and the two upstream parameters \hat{D}_∞ and ψ_i , making a total of five dimensionless numbers. In the present formulation, the volume flux is Q , the dimensional flow variable is h_0 , the geometric variables are L and ΔH , and the upstream variables are H and H_r . These six variables along with f and g , and using the hydrostatic approximation, can define five dimensionless parameters which relate scaled volume flux to the five variables given above. This is the same number as Gill's. However, (2.12) has only four dimensionless numbers. The scaled flux is easily seen to be $2Qf/gH^2$ and this is a function of the three dimensionless parameters ($\gamma, \delta, L/R$) rather than four parameters. The decrease in the number of dimensionless numbers has come about because the geometric parameter ΔH is always subtracted from the flow parameter H_r in this formulation. Because of this, their difference produces only one dimensionless number. This feature has apparently not been previously noted. It produces a useful simplification in the way the solutions can be presented.

Before presenting calculations of volume flux, a better scale for vertical depths than H will be considered. Since velocity in the passage cannot be imaginary, $h_0 \leq H_r - \Delta H$. Defining

$$\eta = H_r - \Delta H - h_0, \quad (2.13a)$$

$$h(-L) = H - (H - H_r + \Delta H + \eta) \cosh(L/R) - \sqrt{2H\eta} \sinh(L/R), \quad (2.13b)$$

makes the formula for volume flux more compact

$$Q = \frac{g}{2f} \left\{ -[(H - H_r + \Delta H + \eta)^2 + 2H\eta] \sinh^2(L/R) + 2H(H - H_r + \Delta H + \eta) [\cosh(L/R) - 1] + \sqrt{2H\eta} [2H \sinh(L/R) - 2(H - H_r + \Delta H + \eta) \sinh(L/R) \cosh(L/R)] \right\} \quad (2.13c)$$

but this is only valid if $h(-L) \geq 0$; otherwise the rapidly rotating limit is recovered

$$Q = \frac{g(H_r - \Delta H - \eta)^2}{2f} = \frac{gh_0^2}{2f}. \quad (2.14)$$

This is maximum for $\eta = 0$. For $L \ll R$, the formula for flux of nonrotating fluid

$$Q = \sqrt{2g\eta}(H_r - \Delta H - \eta)L \quad (2.15)$$

is recovered from (2.13c). This is maximum for $\eta = 2/3(H_r - \Delta H)$.

Both (2.14) and (2.15) have maximum flux depending upon Bernoulli elevation above the passage floor $H_r - \Delta H$ rather than either H_r or H . Moreover, H obviously does not govern the wave speed in the control section as directly as $H_r - \Delta H$. This suggests the use of $H_r - \Delta H$ as a depth scale for volume flux rather than upstream depth so we find that Eq. (2.12) becomes:

$$\begin{aligned} Q^* &= \frac{2fQ}{g(H_r - \Delta H)^2} \\ &= h_0^{*2} - \left[\frac{1}{1-\delta} - \frac{1}{2} \left(\frac{1}{1-\delta} - h_0^* + \sqrt{\frac{2(1-h_0^*)}{1-\delta}} \right) e^{L/R} \right. \\ &\quad \left. - \frac{1}{2} \left(\frac{1}{1-\delta} - h_0^* - \sqrt{\frac{2(1-h_0^*)}{1-\delta}} \right) e^{-L/R} \right]^2, \end{aligned} \quad (2.16a)$$

where

$$h_0^* = h_0 / (H_r - \Delta H). \quad (2.16b)$$

The use of $H_r - \Delta H$ for depth scale rather than either H_r or H is in accord with the flux laws of a number of earlier results. For example there is the result by Killworth and McDonald (1993) that $Q^* = 1$ is an upper limit. This is based on a maximum bound for flux through a passage for arbitrary potential vorticity and arbitrary passage bottom profile. The greatest flux found by Whitehead *et al.* (*loc. cit.*) for zero potential vorticity ($\delta \rightarrow 1^-$) is also $Q^* = 1$. And finally, this is the magnitude of greatest scaled flux for calculations of constant potential vorticity flow where there is no volume flux on the right-hand upstream wall so that $H_r = H$ (Whitehead, 1989).

Calculations of volume flux are shown in Figs. 3 and 4. These show that the results collapse to a few simple curves. In addition, some results

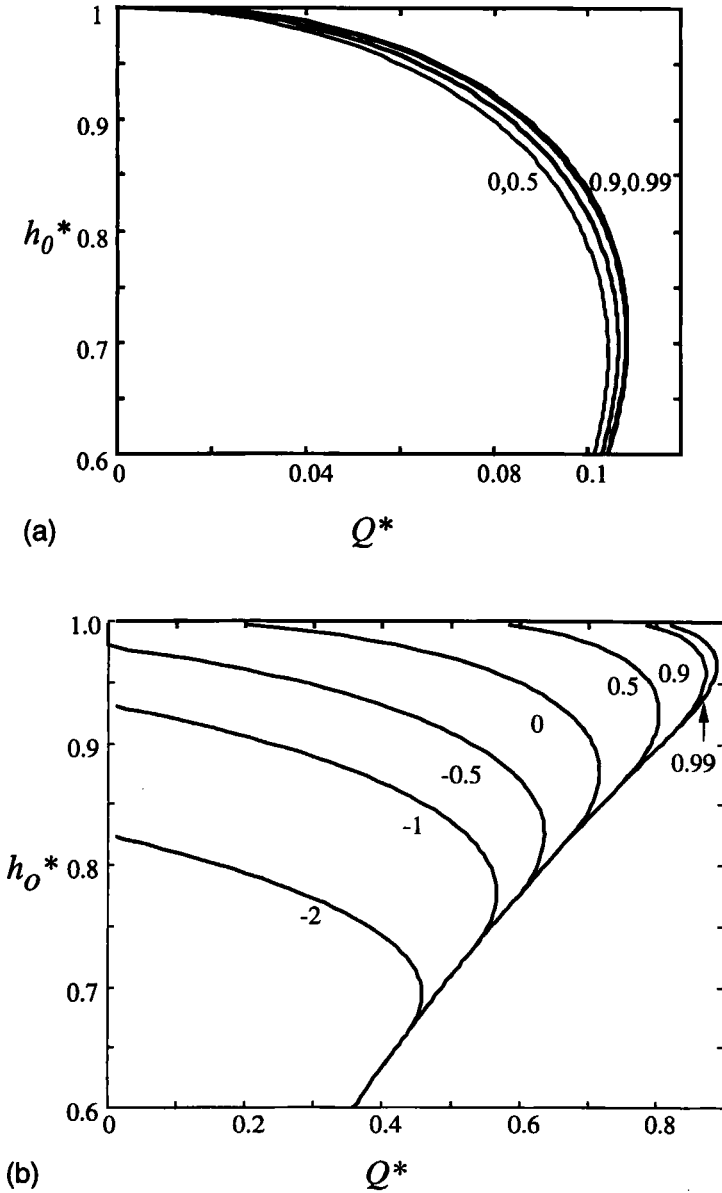


FIGURE 3 Curves of normalized volume flux versus normalized depth at the right-hand wall in the control section. Values of δ are labeled on the curves. (a) Scaled width $L/R=0.1$. (b) Wider control section $L/R=1.0$. (c) Very wide control section $L/R=1.5$. (d) Very large negative values of δ with $L/R=1.0$.

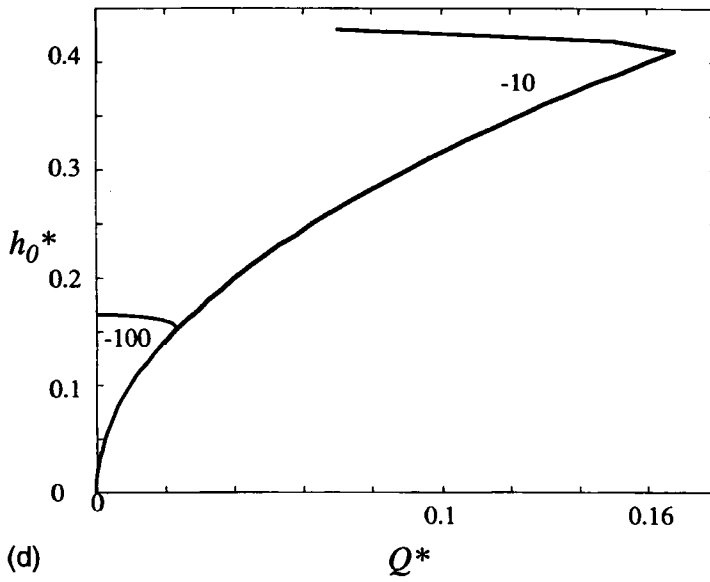
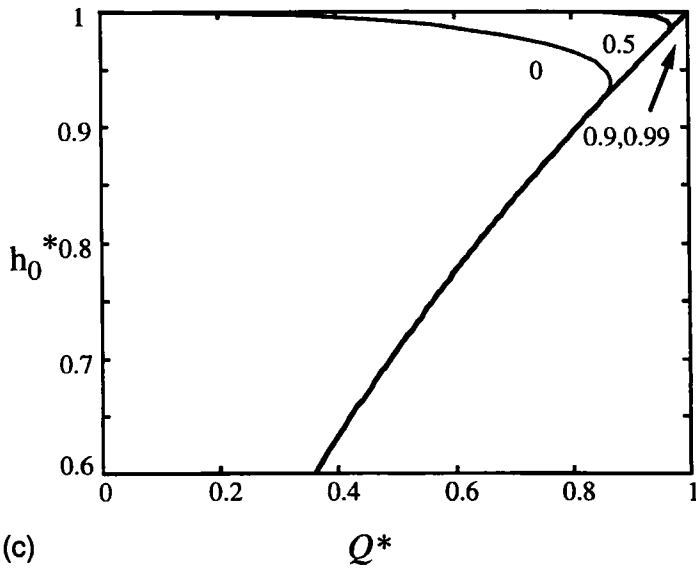


FIGURE 3 (Continued)

with negative δ are new. We chose to vary the free parameter h_0^* . The critical value that produces maximum flux is to be called h_{0c}^* .

Figure 3 contains curves of Q^* calculated over the range $0.6 < h_0^* < 1$ for a number of different passage widths. Panel (a) shows flux for a narrow passage with a scaled width of $L/R = 0.1$. The profiles are for the values $\delta = 0, 0.5, 0.9$, and 0.99 . It is obvious that the various curves of Q^* differ by only a few percent. For $\delta = 0.99$ the upstream depth is 100 times greater than the stagnant depth of water in the passage, so that the approximation of zero potential vorticity is extremely well approximated. Results with the present scaling cluster to within about 5% of each other, and all attain a maximum flux at a value of $h_{0c}^* \cong 0.7$. This value is close to $2/3$, the critical value for Eq. (2.15). Calculations for a channel much narrower than the Rossby radius were made with $L/R = 0.01$ and in the range $0 \leq \delta \leq 0.99$. Results were indistinguishable from (2.15) within 1%.

Figure 3b shows results for a passage as wide as a Rossby radius ($L/R = 1$). It has seven curves in the range $-2.0 < \delta < 0.99$. Results for positive δ are described first. The profiles have maximum values of scaled flux within 20% of 1.0. This vindicates the scaling used for the vertical length scale. The range of h_{0c}^* is ($0.86 < h_{0c}^* < 0.94$) which is larger than for a narrow opening as in Fig. 3a. For $\delta > 0$ critical (maximum) volume flux changes by less than 25%. Although δ is not a large factor in determining volume flux in this range, velocity and height profiles across the passage (not shown) differ with δ . The variation of the profiles with dimensionless numbers was illustrated by Gill (1977). For a wider passage (Fig. 3c) the maximum flux is found for $h_0^* > 0.95$ with $\delta \geq 0$. Magnitude of the scaled flux is within 15% of 1.0.

Negative values of δ are not discussed widely in previous studies. In Figs. 3b and 3d the profiles with negative δ have a range of negative flux near $h_0^* = 1$ (where $v_0 = 0$ from (2.8)). This reverse flow is produced by cyclonic shear in the passage near the right-hand wall as follows: At $h_0^* = 1.0$ there is zero velocity at the right-hand wall so there is always some negative flux near the wall for $\delta < 0$. The values of negative flux are deleted from the curves in Figs. 3b and d, but they can be imagined as extensions to the left of the shown curves. As h_0^* is decreased from a value of one, velocity at the wall is directed downstream and volume flux becomes less negative. The

volume flux becomes positive everywhere at some smaller value of h_0^* and it also attains a maximum as in the previous examples. Figure 3d shows calculations for the extreme values of $\delta = -10$ and $\delta = -100$. Flux is very much smaller than that shown in Figs. 3b and 3c, and h_0^* is less.

Note that from the first line in Eq. (2.12) the criterion for negative total flux is that $h(-L) > h_0$. Using this with (2.13a,b) and with $\eta = 0$, gives the criterion for reverse flux and it reduces to $(H_r - \Delta H - H) \cosh(L/R) > H_r - \Delta H - H$. Since $\cosh(L/R) \geq 1$, this requires that both sides are positive which in turn requires that $\delta < 0$. Two separate factors in the upstream region can contribute to producing $\delta < 0$. One factor is the presence of a current next to the right-hand upstream channel wall so that $H_r > H$. For example, a pump feeding additional fluid along this channel wall will pile up fluid and make a current flowing toward the passage. This accumulation both makes Bernoulli potential greater and produces a current with positive shear even in the upstream basin. The second factor is a deeper bottom in the passage than upstream, so that $\Delta H < 0$. This produces cyclonic shear by vortex stretching of columns as they travel from the channel to the passage. Both influences must add together to make $\delta < 0$.

Below the maxima in Fig. 3 panels b–d the curves merge. This indicates that the interface intersects the bottom of the passage. For two of the values of δ in Fig. 3c, the interface depth at $x = -L$ is negative for all values of h_0^* so that $h_0^* = 1$ itself produces intersection with the bottom. The criterion for critical flow in the case where the interface intersects the bottom is $\eta = 0$ from (2.14). This can be used with a criterion requiring intersection with the bottom that is found by setting $h = 0$ in (2.11a). The combination yields the following simple criterion for intersection of the bottom with maximum flow:

$$\cosh(L/R) > \delta^{-1}. \quad (2.17)$$

This implies that for $\delta = 0$ the value of L is infinite. This is a special case that was previously noted to be true for a flat bottom, i.e. $\Delta H = 0$ (Gill, 1977). However, it was noted only for the example with no current along the right-hand wall. With upstream currents

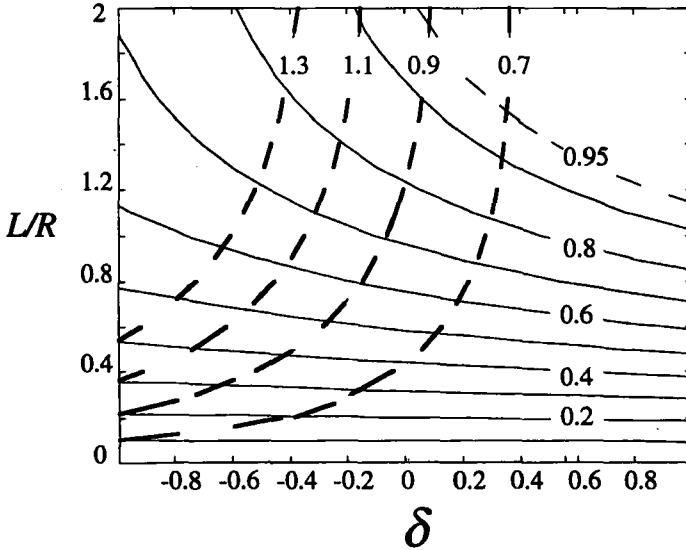


FIGURE 4 Contours of volume flux as a function of scaled channel width L/R and δ . The dashed lines to the left denote limits to the calculation from Eq. (2.19) for four values of r shown. To the left of the dashed lines the upstream channel is unable to supply fluid to the passage.

of any magnitude the complete criterion for which there is no intersection for all passage widths is $\delta > 0$ so that the upstream conditions are

$$H + \Delta H - H_r > 0. \quad (2.18)$$

Contours of scaled flux are shown as a function of δ and L/R in Fig. 4. We see that the effects of the variation of the parameter δ are most pronounced for wide passages. Can the values of Q^* shown in Fig. 4 be satisfied for all upstream channel flows? This requirement is readily calculated by setting flux less than the maximum total volume flux toward the passage in the upstream channel which is given setting the fluid elevation at the left-hand wall to zero, so that $Q_{\max} = gh_{ur}^2/2f$. Using Eq. (2.7) this becomes

$$Q^* < Q_{\max}^* = (2r - 1)(1 - \delta)^{-2}. \quad (2.19)$$

This introduces the dimensionless parameter $r = H_r/H$. The criterion given by (2.19) is shown as dashed curves. Above and to the left of

these curves, the upstream cannot supply enough volume flux for values given by the contours. Therefore in these cases the flux is limited by the flow in the upstream basin. The free surface intersects the bottom of the infinitely wide channel and has a maximum value there. The flow in the passage cannot be a maximum value and thus would be subcritical.

It is clear from (2.7) that the strength of the right-hand upstream boundary layer varies with the value of r . This fact brings the present formulation to agreement with Gill's formulation that contains three dimensionless numbers needed to specify the conditions upstream. The significant difference between the present choice in dimensionless variables and Gill's is that r is not required to determine the properties of flow at the passage.

Since both the maximum flux is specified for fixed δ and L/R and the strength of the right-hand upstream boundary layer varies with the value of r , the strength of the left-hand upstream boundary layer must also vary with the value of r . In addition, ΔH varies with the value of r for fixed δ and L/R . It is then obvious that there is a range of r (and thus a range of upstream flows) that produces the same point in Fig. 4.

To illustrate a variety of upstream flows for the same passage flow, we pick the parameters $\delta = 0.2$ and $L/R = 1$ for which $Q^* \cong 0.75$. The relation between upstream height on the walls and the parameters are then found first by using (2.7)

$$h_{ur}/H = \sqrt{2r - 1}, \quad (2.20)$$

second by using the upstream relation for volume flux

$$h_{ul}/H = \sqrt{2r - 1 - (1 - \delta)^2 Q^*}, \quad (2.21)$$

and third by using the definitions of the dimensionless numbers

$$\Delta H/H = \delta + r - 1. \quad (2.22)$$

For simplicity, an example with $Q^* = \frac{3}{4}$ is shown in Fig. 5. It shows the profiles of the left and right-hand upstream surfaces for five values of r . The rectangular passage along with the maximum flux surface profile is the same for all these cases. This is included in the middle

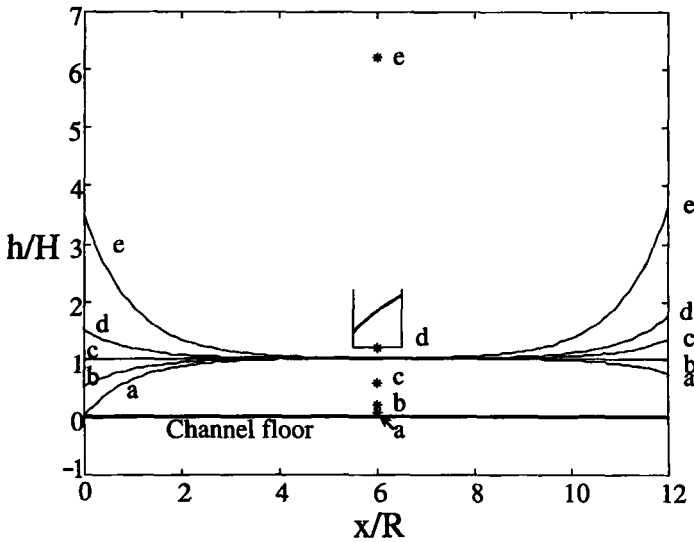


FIGURE 5 A range of upstream surface profiles for various values of r . These all create the same exit profile shown in the center. For this case, $L/R = 1.0$, $\delta = 0.2$ and (a) $r = 0.875$, (b) $r = 1$, (c) $r = 1$, (d) $r = 2$, (e) $r = 7$.

of the figure. Also shown by stars are elevations of the floor of the passage above the upstream channel for each case. The smallest possible value is $r = 0.875$. For this, both of the currents on the sides of the channel are currents of depression, and the current on the left-hand upstream channel is touching the bottom. Fluid on the left-hand wall flows toward the passage and fluid on the right-hand wall flows away from the passage. The floor of the passage is 0.075 times H above the channel floor. The next value is $r = 1$, ($H_r = h_{ur} = H$). There is no current on the right-hand wall. Passage floor elevation is 0.2. In contrast, for the next value $r = 1\frac{3}{8}$ there is no current on the left-hand wall. Passage floor elevation is 0.575. For $r = 2$ both currents are currents of elevation. Fluid flows toward the passage along the right-hand wall with volume flux of 2. Some fluid also flows away from the passage along the left-hand wall. For $r = 7$ the currents are simply greater than those of with smaller r . Scaled elevation of the floor of the passage is 6.2, a value greater than the maximum height on the right-hand wall in the upstream basin of magnitude 3.6.

Scaled flux along the right-hand wall has a magnitude of 11.96. The only way for the fluid to attain the elevation of the channel is for some of the fluid to be raised to the level of the channel by the Bernoulli potential of the right-hand current. The picture of very rapid right and left-hand currents continues for all greater values of r .

All the upstream channel flows are subcritical even though $h_{ur} \gg 1$, $h_{ul} \gg 1$ for $r \gg 1$. It is simple to determine that all such upstream currents are subcritical using Eq. (3.20) of Pratt (1983). In the limit of infinitely wide upstream channels the Froude number becomes $|h_{ur} - H|/(h_{ur} + H)$ and $|h_{ul} - H|/(h_{ul} + H)$ for the right and left-hand currents, respectively. These values are always less than one since all heights are positive.

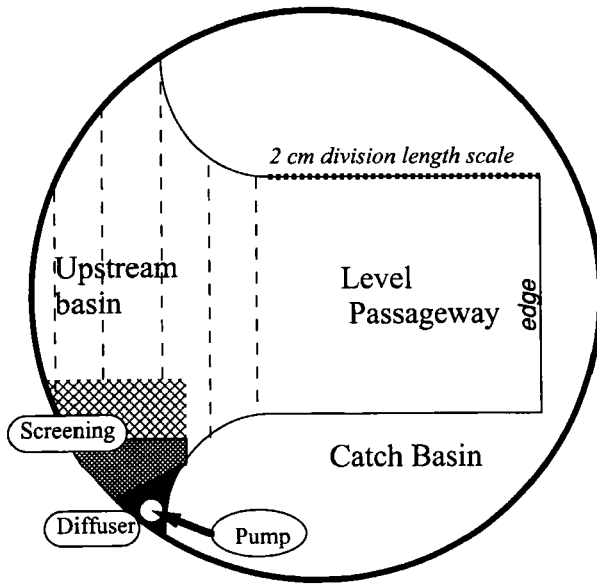
3. EXPERIMENTAL OBSERVATIONS OF CONSTANT POTENTIAL VORTICITY FLOWS

Laboratory observations of flow upstream of critically controlled rotating flows are scanty. For a long passage with level depth they consist of three laboratory studies (Whitehead *et al.*, 1974; Shen, 1982; Borenas and Whitehead, 1998). Only the last study measured some aspects of the velocity profile near and upstream of the control section. A closed gyre is located upstream of the control point, a feature in accordance with the accompanying semi-geostrophic theory. This feature can be found with the present equations by letting ΔH go smoothly to zero between upstream and the control section. But the nature of currents further upstream is still unknown. Most ocean studies (summarized by Whitehead, 1989, 1998) do not contain CTD sections across the upstream channel that reveal the distribution of upstream currents. The following experiment was made to see upstream flows and to measure velocity distribution at the sill.

3.1. Apparatus

The primary objective was to clarify the nature of flows upstream of a controlling passage. Experiments were conducted using one layer of water under air over a very flat bottom on a rotating turntable as

TOP VIEW



SIDE VIEW

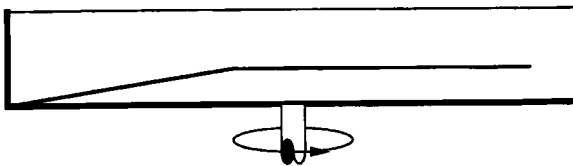


FIGURE 6 Sketch of the laboratory apparatus.

sketched in Fig. 6. Water flowed from a smooth and deeper upstream basin into a level passage. The water spilled from that into a catch basin over a sharp edge with the intent that at some point of the passage a critical point would form. The experimental apparatus consisted of a 2-meter diameter cylindrical container fixed to a rotating turntable with a vertical axis of rotation. A glass plate 74 cm wide and 96 cm long served as the bottom of the passage. It was crucial that this be very flat and level. The former was served well by plate glass which is flat, except for sagging from its own weight and the weight of water above it, to better than 0.01 cm through a combination of

its own strength and reinforcement. The latter was accomplished by leveling to within 0.07 cm/meter using a tripod arrangement of adjustable vertical legs, measurements being taken with a precise level. The container was full of water to experimental depth to compensate for any compression of the bottom of the large fiberglass tank. An upstream basin was constructed of thin acrylic and PVC plastic sheet. Contours of the bottom and sidewalls were constructed of smooth curves, and the bottom slope of the upstream region was fixed at 10 degrees. Sidewalls were adhered to the sloping bottom and plate glass after the glass plate was leveled to ensure precise leveling, although the level was carefully checked after construction was complete. The bottom and sidewalls were made smooth with filler material to eliminate abrupt edges. In the catch basin a submerged impeller pump with a flow rate of $4.2 \times 10^{-4} \text{ m}^3 \text{ s}^{-1}$ was used as the fluid source.

Water entered the upstream region via flexible tubing; with the outlet end of the tubing imbedded in open cell foam with pore sizing of 14 pores cm^{-2} . The length of tubing inside the foam was made large enough for the flow to seep uniformly out of the foam through all surfaces. A rough porous false bottom of layers of stainless steel screening was constructed over the deep upstream bottom in a peripheral region surrounding the foam source for a distance of roughly 20 cm. The thickness of this region was more than 1 cm deep near the source, and comprised of five layers of screen, but the number of layers and thus the thickness was tapered to zero at the edge of the region. This attenuated any eddies produced by concentrated currents near the source, so there was a large diverging water source with relatively uniform outflow around this region. The source was located at four different positions in the upstream basin. The first location was at the right-hand wall and produced the flows of greatest interest. The second was in the middle of the upstream basin not in contact with any wall, the third was in the middle of the upstream basin in contact with the outer wall of the tank, and the fourth was at the left-hand wall. At the outer end of the passage, the water spilled into the catch basin. This basin was located below and around the glass-bottomed passage, bounded by the outer walls and bottom of the cylindrical tank, and filled with the working fluid—water dyed black.

Measurements were taken after the turntable was brought to steady rotation, accurate to better than one percent. The pump was then turned on and upstream height increased until water began to flow over the level passage, which was painted white so that small or zero water thickness was obvious. Velocity observations were determined by using white polyethylene spheres placed onto selected regions of the upstream basin and subsequently floated along the water surface to mark the current. The pellet trajectories were recorded both on video and with streak (time-lapse) photographs. It would typically take fifteen to twenty minutes for the upstream flow to settle down to what appeared to be its asymptotic long-time configuration.

Few experiments have produced rotating critically controlled flow using a layer of water under air. Some previous experiments have used the air-water experiment to investigate flows and the hydraulic jump downstream of a control point (Pratt and Lundberg, 1991) or with other geometries (Whitehead and Porter, 1977; Whitehead, 1986). Previous experiments investigating hydraulic control (Whitehead *et al.*, 1974; Shen, 1982; Borenas and Whitehead, 1998) have always used two layers with fluids of different density which, in virtue of producing a reduced gravity, made local Rossby Radius as small as centimeters in size. Thus it is important to give estimates of the governing parameters to illustrate why this experiment was expected to work.

With water under air, the height of the upstream fluid above the floor of the passage on the right-hand wall is found using (2.14)

$$h_0 = \sqrt{\frac{2fQ}{g}}. \quad (3.1)$$

Using the values $g = 9.8 \text{ ms}^{-2}$, $Q = 4.2 \times 10^{-4} \text{ m}^3 \text{ s}^{-1}$, and the three values $f = 0.5, 1.0, \text{ and } 2.0 \text{ s}^{-1}$ respectively, $h_0 = 0.0065, 0.0091, \text{ and } 0.013 \text{ m}$, respectively. Rossby Radius based on that depth is given by

$$R_l = \sqrt{\frac{gh_0}{f}}, \quad (3.2)$$

and has the values $R_l = 0.50, 0.30, \text{ and } 0.18 \text{ m}$, respectively. Since passage width is greater than those values, the rapidly rotating

predictions of rotating hydraulic theory can be tested. However, the layer thickness is small enough so that viscous drag might be important. To assess this possibility, note that the velocity scale is

$$v_s = \sqrt{gh_0} \quad (3.3)$$

which is $v_s = 0.25, 0.30,$ and 0.36 m s^{-1} , respectively with the above values.

Thus a water particle will traverse the 0.96 m passage in about 3 or 4 s, although some water will go slower than this and the traverse time will be accordingly longer. The spin-down time due to Ekman drag is

$$t_d = \frac{h_0}{\sqrt{vf}} \cong 9.2 \text{ s}, \quad (3.4)$$

an interval longer than the traverse time scale. Thus there is some hope that viscous drag plays a small role, although clearly it is not negligible everywhere.

Centrifugal force will cause the surface of motionless water d_0 to assume a parabolic shape according to the formula $d_0 = \Omega^2 r^2 / 2g$. Values of $d_0 = 0.01 \text{ m}$ are found at radii of 1.8, 0.9, and 0.45 m for $f = 0.5, 1.0,$ and 2.0 s^{-1} , respectively. The deflection is comparable to transforming the flat passage bottom into an inverted parabola. Thus the shallowest point is at the exact center of rotation surrounded by circular contours of greater depth. The runs with $f = 0.5$ and 1.0 s^{-1} have depressions of $d_0 = 0.00625$ and 0.0025 m at the 0.45 m radius and are judged to be more strongly effected by geostrophic effects rather than centrifugal force. The results with $f = 2.0$ probably have an equal influence of each. But in all cases, the control point should be located close to the center of rotation.

3.2. Qualitative Observations

Experiments were conducted for rotation rates of $f = 0, 0.5, 1.0,$ and 2.0 s^{-1} giving $L/R_l = 1.4, 2.5,$ and 3.9 respectively for the rotating experiments. The experiment for $f = 0$, was run to see if the geometry was smooth, flat, and level enough to produce a uniform out-flow along the passage. Videotape images reveal that the flow was reasonably uniform in the region where the water ascended the sloping

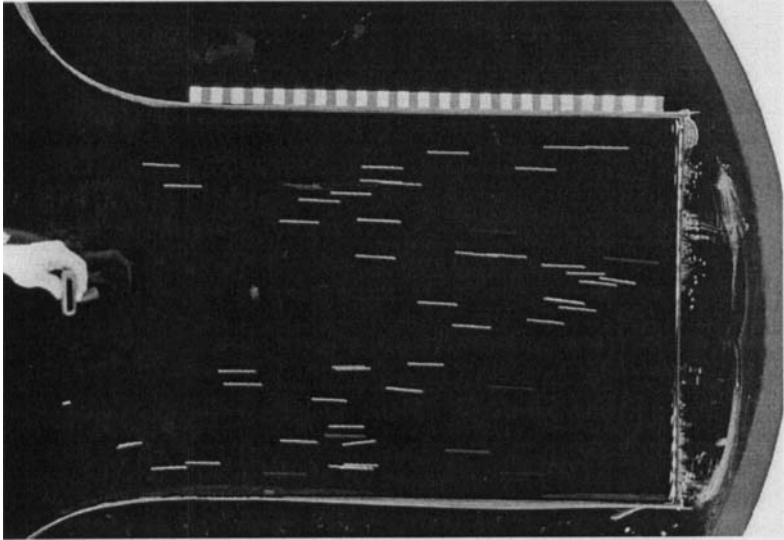


FIGURE 7 Streak photographs of floats in the passage for zero rotation. Time interval is 0.5s.

bottom to the level passage. Outflow in the passage was uniformly spread out across the passage as shown in Fig. 7.

For all source locations with rotation, the water in the upstream basin had a distinctive flow pattern that differed with rotation rate only in small details as described at the end of this section. This pattern is most clearly illustrated for all three values of rotation with the source at the right-hand wall in Fig. 8. The current emerged from the source and flowed directly from the upstream right-hand wall to the left-hand wall (bottom to top in the photographs) parallel to the sloping bottom contours. A constricted, tightly curving current ascended the sloping bottom near the left-hand wall. Over the level region the current was pointed to the right of the axis of the passage and crossed to the right-hand wall of the passage.

There were two regions of very slow (almost stagnant) flow on both sides of the upstream current. One lay over the deepest part of the upstream basin to the left of the current that moves from right to left in the upstream basin. The second was to the right of the curving current ascending the sloping bottom. It lay mostly over the right-hand sloping bottom region, although there was a little stagnant

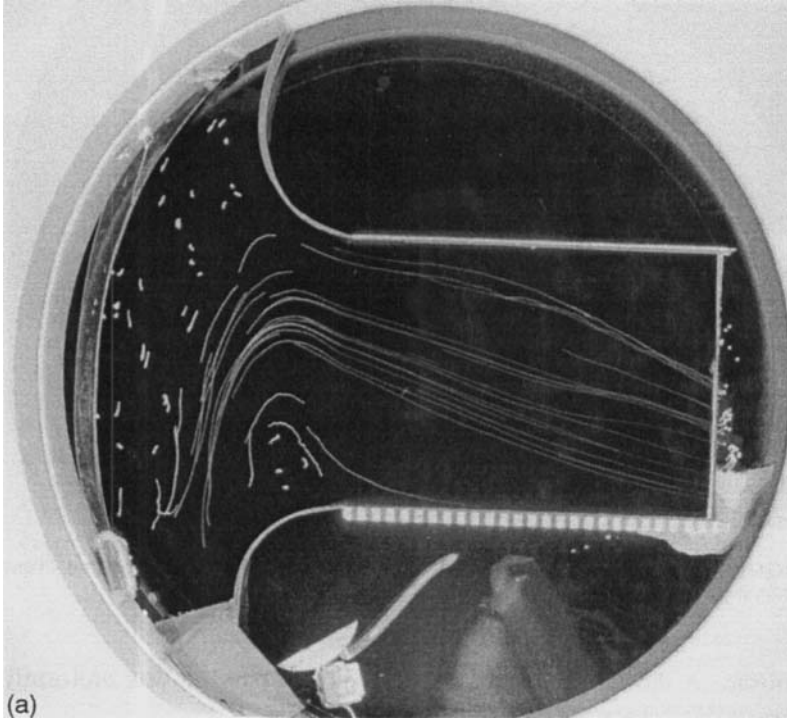


FIGURE 8 Streak photographs of floats in both the upstream and controlled region. (a) $f = 0.5 \text{ s}^{-1}$, $L/R = 1.25$. (b) $f = 1.0 \text{ s}^{-1}$, $L/R_f = 2.5$. (c) $f = 2.0 \text{ s}^{-1}$, $L/R_f = 5$.

water on the level passage as well. It resembles the gyre upstream of the control point studied in a straight passage by Borenas and Whitehead (1998).

As the current proceeded along the level passage (Fig. 9), each streamline was approximately straight for the moderate rotation experiments but tilted toward the right-hand wall. Streamlines that were thereby forced into the right-hand wall veered and became aligned with the wall. To the left of the large current in the flat passage was a thin layer of water that we believe to be about an Ekman layer thick. The white bottom is visible through this thin layer in some panels. The water in this thin layer had steady uniform flow from the edge of the large current to the end of the passage. Injected dye revealed that the flow was directed at a different angle to the main current,

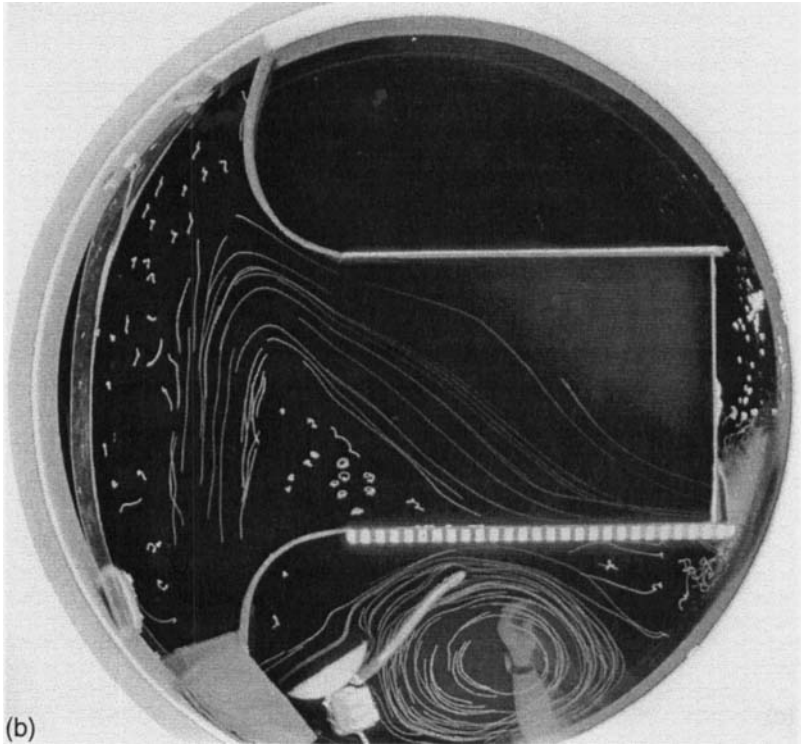


FIGURE 8 (Continued)

but detailed measurements in this thin current have not been made. We anticipated that this has an Ekman layer whose resolution required instruments not available at the time. For $f > 0.5 \text{ s}^{-1}$ the stagnation regions over the sloping bottom were much larger than the counterpart with slower rotation.

For a flow rate of $f = 2.0 \text{ s}^{-1}$ (Figs. 8c and 9c) the upstream current flowing from the right-hand wall to the left-hand wall over the sloping bottom penetrated further to the left than previously. It then curved to the right in a much more tightly curved and narrower arc near the left-hand wall. The stagnant region to the right of the curving current was much larger than the previous cases. The current over the flat passage was directed more toward the right-hand wall than toward the exit. Thus this current impacted into the sidewall and formed a pronounced time-dependent current. We interpret this as a hydraulic jump that

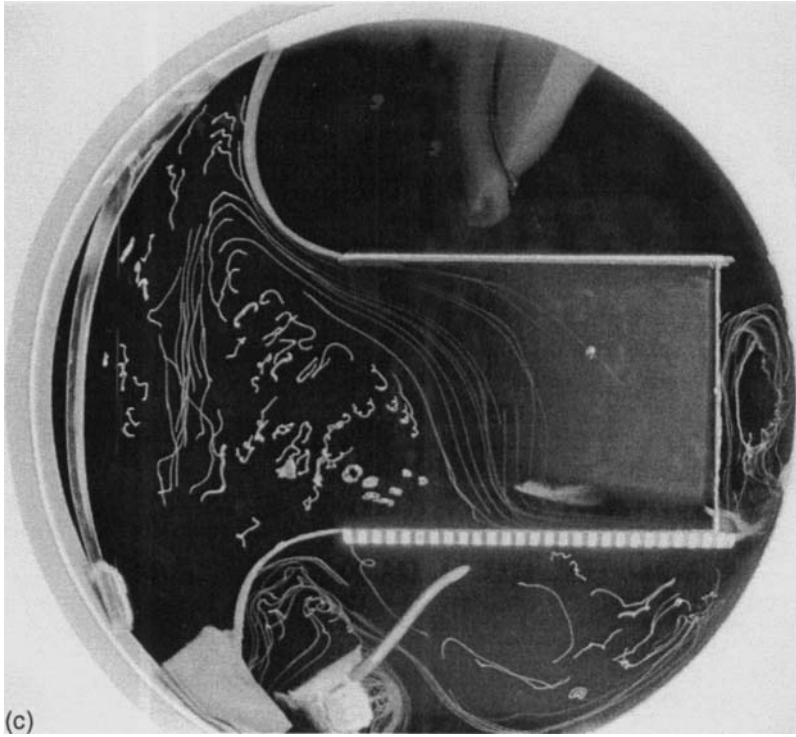
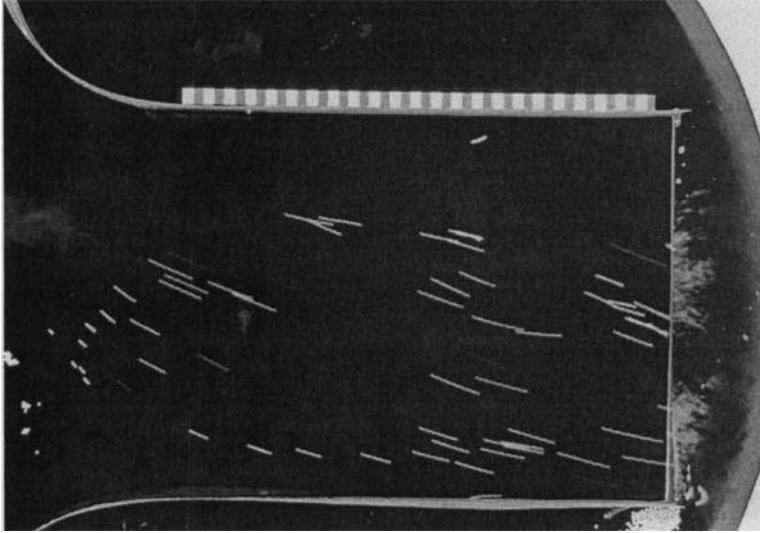


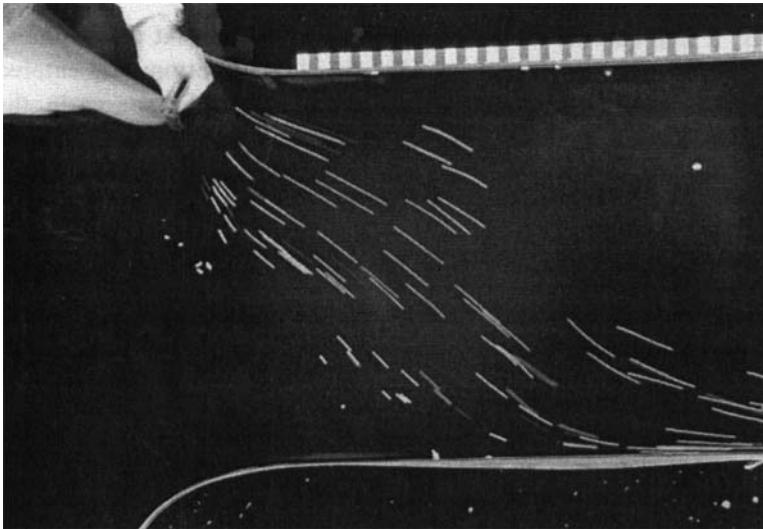
FIGURE 8 (Continued)

stood off the wall as a shock aligned with the sidewall. The picture of the impacting current and the shock region is closely in accord with the picture by Pratt (1987). Around and downstream of the shock a strong narrow localized current formed at the right-hand sidewall of the passage about midway along the passage where the curving current impinged onto the wall. Turbulent appearing fluctuations were frequently visible at the left-hand edge of this localized current on videotapes. The region with a thin layer of water was also quite large and covered most of the downstream half of the flat passage.

With source locations in the other three places, currents also flowed to the left-hand corner of the upstream basin. With the source in the middle of the upstream region the current circulated counterclockwise (as required by angular momentum conservation) around the source so that particles spiraled outward. At the outer wall of the cylindrical

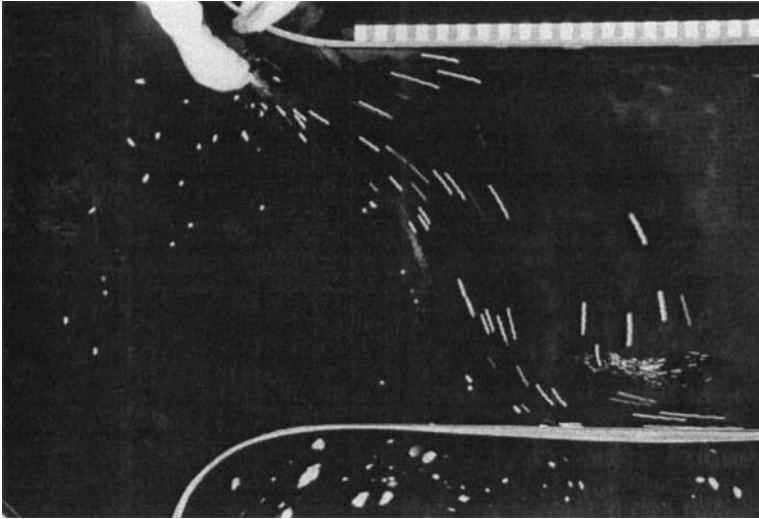


(a)



(b)

FIGURE 9 Streak photographs of floats in the controlled region. Time interval is 0.5 s except for case (c) which has 0.25 s. (a) $f = 0.5 \text{ s}^{-1}$, $L/R_l = 1.25$. (b) $f = 1.0 \text{ s}^{-1}$, $L/R_l = 2.5$. (c) $f = 2.0 \text{ s}^{-1}$, $L/R_l = 5$.



(c)

FIGURE 9 (Continued)

tank, a wall current formed which went to the left. At the left-hand upstream corner the water ascended the sloping bottom and entered the level passage near the left-hand wall. With the source in the middle of the outer wall of the tank, the flow went to the left in the upstream basin and entered the level passage near the left-hand wall. With the source near the left-hand wall, the current flowed directly up the slope into the level passage. All source locations produced currents in the level passage that visually appeared to be identical to the counterparts shown here. In addition the region corresponding to gyres was of similar size.

3.3. Quantitative Measurements

Streak photographs such as those shown in Figs. 7–9 were obtained after the steady flow had become fully established with upstream source on the right-hand wall. Care was taken to obtain clear and unambiguous streaks for all the particles so that information would not be skewed by the neglect of some streaks. The streaks were digitized from these and additional photographs.

Naturally one expects little shear for the flow without rotation, and that is clearly true in the digitized data in Fig. 10. With rotation, (Figs. 10b, c and d) there is a current flowing roughly in a straight line at some angle to the axis of the passage. Since we desired to

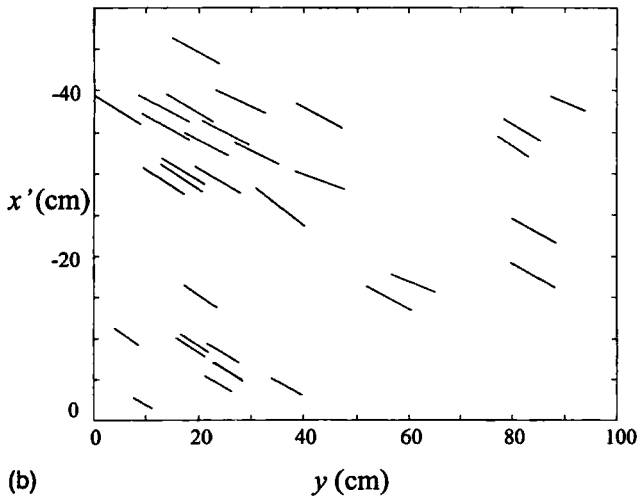
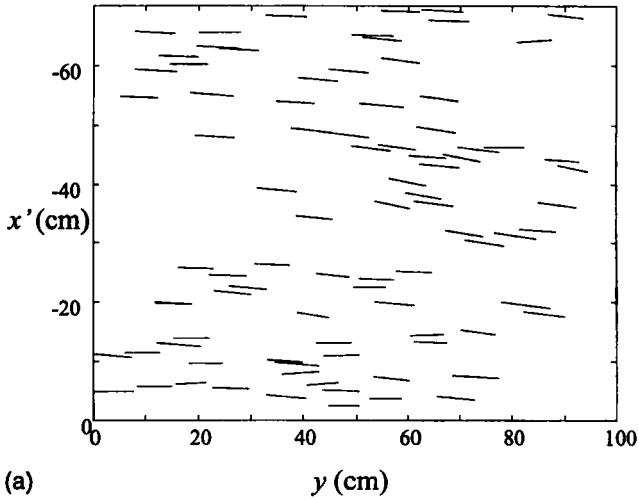


FIGURE 10 Digitized streaks in the controlled regions. (a) $f=0$. (b) $f = 0.5 \text{ s}^{-1}$, $L/R_t = 1.25$. (c) $f = 1.0 \text{ s}^{-1}$, $L/R_t = 2.5$. (d) $f = 2.0 \text{ s}^{-1}$, $L/R_t = 5$. (e) Streaks from case (b) rotated to lie in the direction of average flow.

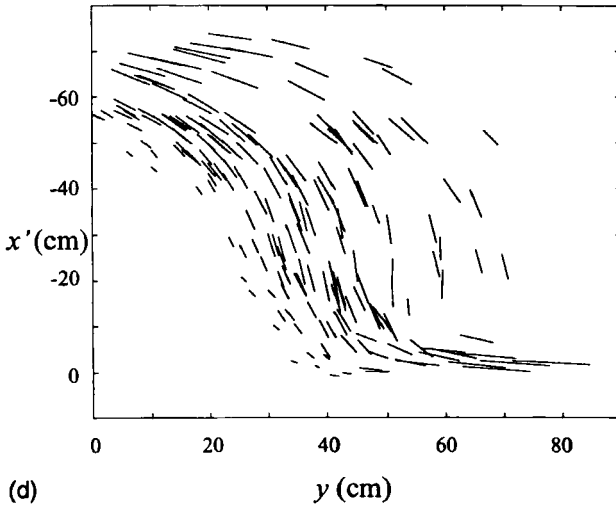
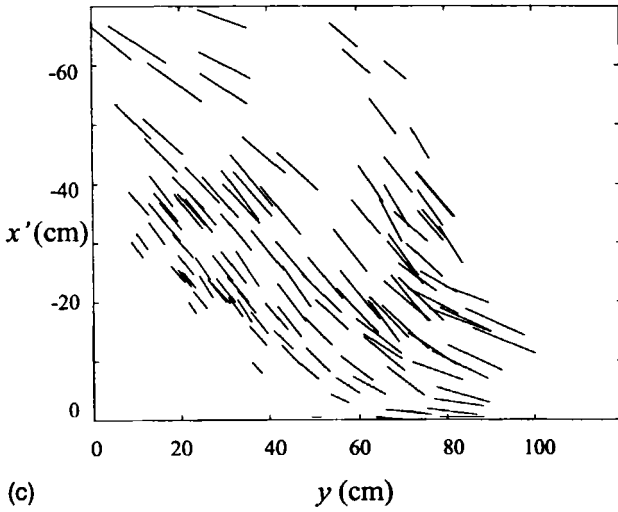


FIGURE 10 (Continued)

attain data perpendicular to the flow direction, we defined the coordinate perpendicular to the sidewall x' in panels a-d. To produce a velocity profile across the current, this current was rotated to a coordinate system with one axis in the flow direction and the other at right angles to the current. The coordinate across the current is defined as

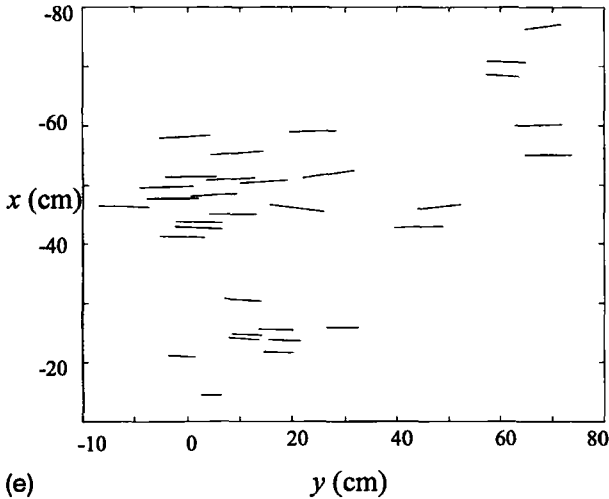


FIGURE 10 (Continued)

x following the notation in Section 2. The average value of the angle was determined for all the streaks in each figure and a geometric rotation of that data set was executed. Such a rotated set is shown in Fig. 10e. From this, length of the streaks was plotted as a function of distance at right angles to the current, assigning an arbitrary value to the zero distance. In this way, velocity profiles were obtained for the four currents by dividing length by time interval. These are shown in Fig. 11a–d.

For the run without rotation (Fig. 11a), the data have a mean velocity of 0.143 m/s with a standard deviation of 0.013 m/s. For inviscid hydraulic control, we consider a passage $L = 0.74$ m wide with a flow rate of $Q = 4.23 \times 10^{-4} \text{ m}^3 \text{ s}^{-1}$. The upstream height and passage velocity for inviscid hydraulically controlled flow is given by

$$H_r - \Delta H = \frac{3}{2}(Q^2/L^2g)^{1/3}, \quad v = \sqrt{\frac{2}{3}g(H_r - \Delta H)} \quad (3.5)$$

which gives upstream height of 0.0049 m and a velocity of 0.18 m/s, a value of almost 30% greater than measurements. We estimate errors in flatness of the glass of about ± 0.001 m, a value in accord with the discrepancy between theory and data. In addition, friction and turbulence

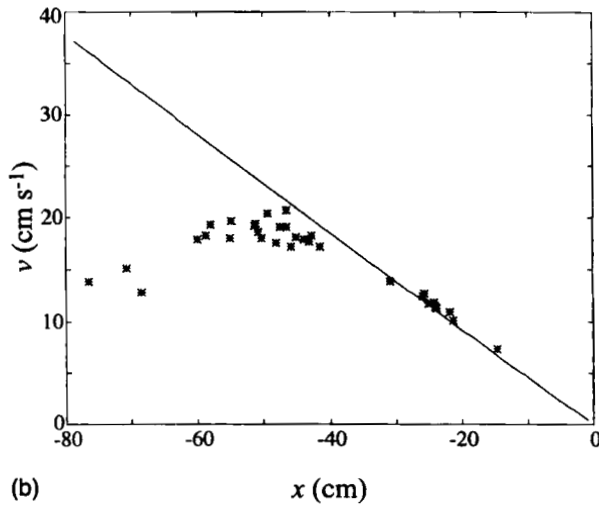
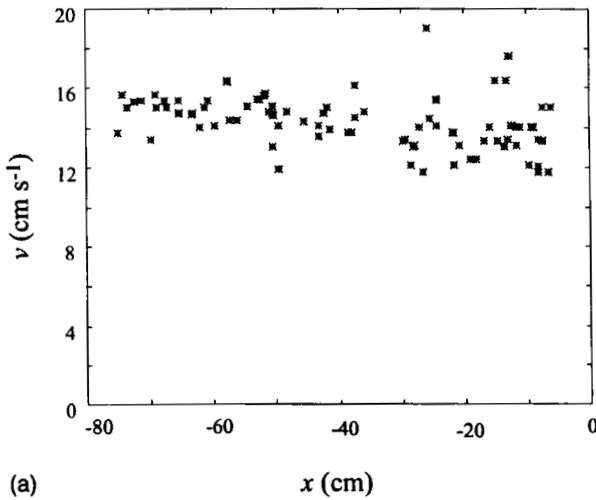


FIGURE 11 Speed versus cross current distance x . (a) $f = 0.5 \text{ s}^{-1}$, $L/R_l = 1.25$. (b) $f = 1.0 \text{ s}^{-1}$, $L/R_l = 2.5$. (c) $f = 2.0 \text{ s}^{-1}$, $L/R_l = 5$. The curves are solutions for Eq. (2.11b) with $H = 0.07 \text{ m}$ and the values for the experiments.

may slow the fluid down. The scatter in the velocity is consistent with turbulence being present.

In Fig. 11 panels b–d a direct comparison is shown between data and a velocity profile from Eq. (2.11a), using $H = 0.07 \text{ m}$, and

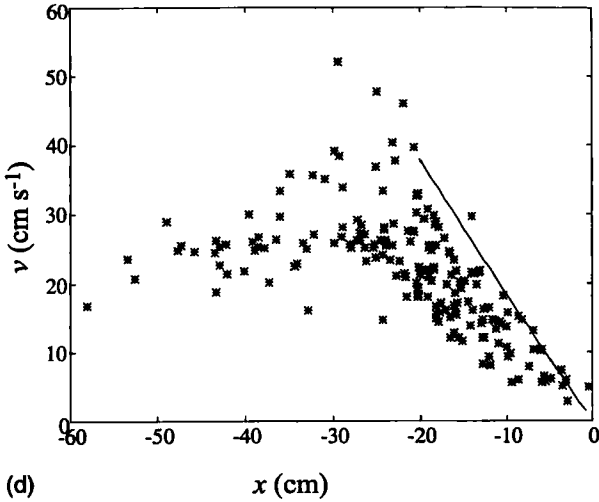
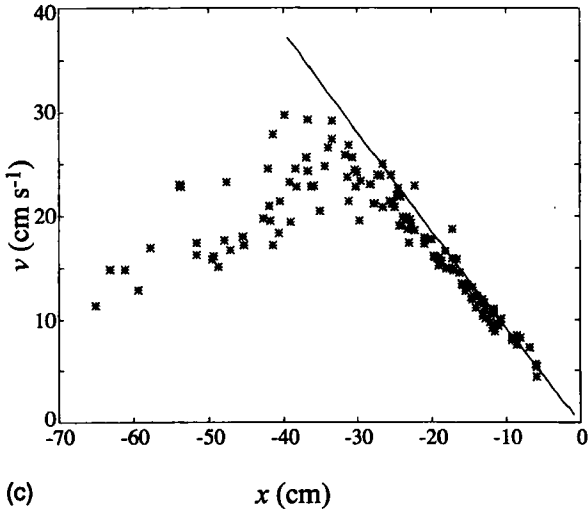


FIGURE 11 (Continued)

$h_0 = 0.0065$ m, and 0.0091 m, and 0.013 m, respectively, as given by (3.1). There is good agreement between data and theory on the right-hand side for Figs. 10b and c, where the shear is approximately constant. The velocity profile curves terminate at the location where the water surface is predicted to intersect the floor. Velocity data

show poor agreement in the vicinity of the termination. In Fig. 11d the data have more scatter on the right and thereby poorer agreement with theory. Figure 10d shows one obvious reason why the fit is so poor. The current is not straight but bends around a curving trajectory. In this case it would be much more appropriate to treat the upstream current in radial coordinates, but no theory is available for direct comparison.

To the left of the constant shear regions are regions in which velocity falls to smaller values but velocity exhibits wide scatter. We interpret the scatter as arising from the edge of the main current where possible meandering is found. Perhaps shear instabilities produce eddies. This region is poorly understood experimentally and theoretically. Probably the counterpart is not resolved in oceanic observations.

Movies in earlier experiments showed that the edge of the current never settled down to completely steady flow (Whitehead *et al.*, 1974, movies akin to their Fig. 3 and caption). It was thought that the instability was of a baroclinic nature (Smith, 1976), although later theory showed that such fronts had a mixed barotropic-baroclinic origin (Griffiths *et al.*, 1982). Our video recordings show similar fluctuations. Virtually the only discussion of the consequences of instability in this region is found in Rydberg (1980). But any fluctuations in the present configuration are certainly barotropic as there is no baroclinic shear so that the nature of eddies at the edge of this current, if they exist, is virtually unexplored.

4. DISCUSSION

Volume flux and profiles of velocity and depth for critically controlled flows in rotating fluid with constant potential vorticity can be determined by specifying two independent upstream parameters. These are upstream depth, and volume flux on the right-hand upstream wall. Two geometric parameters of the passage are also required: the shoaling of the bottom, and passage width. It is shown that all features of flow in the passage depend on the parameter $H_r - \Delta H$. This results in two dimensionless numbers to describe flow in the passage. For example, the volume flux scaled by $g(H_r - \Delta H)^2/2f$ is a function of δ and L/R in Fig. 4. Upstream flows still depend on

three dimensionless parameters, so that a range of upstream flow distributions produces identical flow in the exit passage. Pratt (1997a,b) also found that a range of upstream flow can be realized by processes not considered in this paper and suitable combinations of the present formulation, with upstream models, seems feasible.

Laboratory experiments with volume flux imposed on the right-hand upstream wall demonstrated considerable adjustment of current in the slope region between the source and the passage. Current on the right-hand side veers to the left along constant depth contours and enters the passage on the left-hand side, but then crosses back to the right hand side near the control section. A large stagnation region to the right of this veering current is observed. Such a stagnation region is known (Borenas and Whitehead, 1998). However, a laboratory and numerical study with flow up a sloping bottom reports topographic westward intensification (Kinder *et al.*, 1986). Such adjustment is also seen in recent numerical studies by Helfrich *et al.* (1999). This may be responsible for the current directed from the right to left over the tilted approach to the laboratory passage.

As mentioned in the introduction, the compelling motivation for this work is to clarify the role of assorted upstream features that might influence our estimates of critically controlled flux in ocean passages. Detailed comparison of the theory of such currents and actual ocean currents is still in a crude stage. Measurements of ocean volume fluxes are compared with estimates from hydraulic theory for eight ocean locations (Whitehead, 1998). To obtain estimates to use with hydraulic theory, the elevation of the interface of water flowing into the passage was estimated as the height above sill depth of the bifurcation depth (the depth where a CTD record upstream of the sill splits from a downstream record). From our new results, we find that a better upstream measurement would be $H_r - \Delta H$ along the right-hand bathymetry. Our present theoretical results indicate that the oceanic estimate of upstream height has an error of size $H_r - H$, that is, the Bernoulli height at the right-hand wall should have been used. It is found that the ocean estimates are greater than measurements by factors ranging from about 30 to 170%. However, possibly some of the error comes from currents flowing away from the passage on the upstream right-hand sloping bathymetry. In addition to the above error, additional possible reasons for the excess are: (1) the influence

of known large-scale currents; (2) friction; (3) assuming a passage with a flat bottom; and (4) other potential vorticity effects and more complicated bottom profiles (Killworth and McDonald, 1993; Killworth, 1994). Figure 4 indicates that small reductions of up to 20% might be found using $\delta \cong 0$ (appropriate for a layer of water upstream of a passage) rather than 1.

The results of this work strongly suggest that ocean volume flux estimates ideally require some measurement of the right-hand upstream current. Note that Fig. 4 shows that for $L/R \geq 1$ volume flux is only significantly less than the scale $g(H_r - \Delta H)^2/2f$ for $\delta < 0$ and that in turn is found only for $r < 1$ from (2.19). The physical way this can be realized is to have currents on the right-hand wall flowing away from the passage. In this case, the upstream current feeding the controlled flow is found along the left-hand wall. This illustrates the need for more information upstream of deep ocean passages.

The laboratory experiment recovered good agreement between theory and a velocity profile at the control section, but it displayed a gyre upstream of the passage. Whether such gyres exist upstream of ocean passages remains unknown. If such features exist, future measurements upstream of passages must take such structures into account.

The approaches used here can be extended in a number of ways. The formulation can be used with more complicated problems, for example multi-layer problems or those with complicated passage bathymetry. Since the upstream conditions are independent of flow rate in the passage, one could numerically integrate (2.1a,b) with bottom profile terms starting with any value of h_0 using (2.8) and (2.9) to determine v_0 .

The experiments utilizing water under air can readily be extended and improved to address more questions. For example, if the upstream region were larger the details of the upstream currents in a flat upstream region could be investigated. The upstream region in this study was narrower than the 50 cm or more which constitutes an upstream Rossby radius of deformation. But in spite of this, the upstream currents were narrower than the Rossby Radius. Possibly their width was governed by topographic beta plane scales. It would be very useful to produce extensive upstream regions, perhaps on larger turntables. One advantage of these experiments that employ

water under air is that good quantitative resolution of the velocity profile is obtained so that complete vorticity balances and internal structure of the boundary layers can be resolved. These issues are important in the subject of rotating hydraulics both in the laboratory and in the ocean. Thus further documentation of flows in the hydraulic jump regions and test of relevant theories also seems feasible. Significant advances in this problem may be realized in combination with numerical techniques. It is hoped to continue studies in such problems.

5. CONCLUDING REMARKS

The central new finding of our formulation is that a transition in "degrees of freedom" between upstream and passage is fundamental in the hydraulics problem with rotation. The experiments, the first with water under air, show that the gyre upstream of a passage is a fundamentally important transition structure between the wider-ranging upstream flows and the more tightly constrained controlled passage flow. The results illustrate the sensitive and important nature of the region immediately upstream of controlling passages. They imply that present observations of ocean flows should be extended further into the upstream regions to determine the nature of the currents flowing into the controlled regions.

Acknowledgements

Support for the theory was provided by a Mellon Award from the Woods Hole Oceanographic Institution, in conjunction with a book project with Larry Pratt, whom we also thank for constructive comments. Support for thoughts and seminars which led to the computations was provided by The National Science Foundation, Physical Oceanography section to the Geophysical Fluid Dynamics Summer Study Program, under grant OCE9314484. Support for the experiment was provided by the Office Of Naval Research under grant N00014-97-1-0195 and during the summer school by grant N00014-97-1-0934. Contribution number 9896 of the Woods Hole Oceanographic Institution.

References

- Armi, L. (1989). The hydraulics of zonal planetary currents. *J. Fluid Mech.*, **201**, 357–377.
- Borenas, K. and Lundberg, P. (1986). Rotating hydraulics of flow in a parabolic channel. *J. Fluid Mech.*, **167**, 309–326.
- Borenas, K.M. and Lundberg, P.A. (1988). On the Deep-Water flow through the Faeroe bank channel. *J. Geophys. Res.*, **93**, 1281–1292.
- Borenas, K.M. and Whitehead, J.A. (1998). Upstream separation in a rotating channel flow. *J. Geophys. Res.*, **103**, C4 7567–7578.
- Dickson, R.M. and Brown, J. (1994). The production of North Atlantic Deep Water: Sources, rates and pathways. *J. Geophys. Res.*, **99**, 12319–12341.
- Dickson, R.R., Gmitrowicz, E.M. and Watson, A.J. (1990). Deep Water renewal in the Northern Atlantic. *Nature*, **344**, 848–850.
- Gill A.E. (1976). Adjustment under gravity in a rotating channel. *J. Fluid Mech.*, **77**, 603–621.
- Gill, A.E. (1977). The hydraulics of rotating channel flow. *J. Fluid Mech.*, **80**, 641–671.
- Girton, J.B. and Sanford, T.B. (1999). Velocity Profile measurements of the Denmark Strait. *International WOCE newsletter*, **37**, 28–30.
- Girton, J.B., Sanford, T.B. and Kase, R.H. (2001). Synoptic Sections of the Denmark Strait Overflow. *Geophys. Res. Lett.*, **28**, 1617–1622.
- Griffiths, R.W., Killworth, P.D. and Stern, M.E. (1982). Ageostrophic instability of ocean currents. *J. Fluid Mech.*, **117**, 343–377.
- Griffiths, R.W. and Hopfinger, E.J. (1983). Gravity current moving along a lateral boundary in a rotating fluid. *J. Fluid Mech.*, **134**, 357–399.
- Hall, M.M., McCartney, M. and Whitehead, J.A. (1997). Antarctic bottom water flux in the Equatorial Western Atlantic. *J. Physical Oc.*, **27**, 1903–1926.
- Haynes, P.H., Johnson, E.R. and Hurst, R.G. (1993). A simple model of Rossby-wave hydraulic behaviour. *J. Fluid Mech.*, **253**, 359–384.
- Helfrich, K.R. Kuo, Allen C. and Pratt, L.J. (1999). Nonlinear Rossby Adjustment in a Channel. *J. Fluid Mech.*, **390**, 187–222.
- Hogg, N.G., Siedler, G. and Zenk, W. (1999). Circulation and variability at the southern boundary of the Brazil Basin. *J. Phys. Oc.*, **29**, 145–157.
- Hogg, N., Biscaye, P., Gardner, W. and Schmitz, W.J. (1982). On the transport and modification of Antarctic Bottom Water in the Vema Channel. *J. Marine Res.*, **40**, Suppl. 231–263.
- Hughes, R.L. (1986a). On the role of criticality in coastal flows over irregular bottom topography. *Dyn. Atmos. Oc.*, **10**, 129–147.
- Hughes, R.L. (1986b). On the conjugate behaviour of weak along-shore flows. *Tellus*, **38A**, 277–284.
- Hughes, R.L. (1987). The role of the higher shelf modes in coastal hydraulics. *J. Mar. Res.*, **45**, 33–58.
- Johnson, E.R. and Clarke, S.R. (2001). Rossby wave hydraulics. *Annu. Rev. Fluid Mech.*, **33**, 207–230.
- Johnson, G.C. and Ohlsen, D.R. (1994). Frictionally modified rotating hydraulic channel exchange and ocean outflows. *J. Phys. Oceanogr.*, **24**, 66–78.
- Killworth, P.D. (1992). Flow properties in rotating, stratified hydraulics. *J. Phys. Oceanogr.*, **22**, 997–1017.
- Killworth, P. (1994). On reduced-gravity flow through sills. *Geophys. Astrophys. Fluid Dynam.*, **75**, 91–106.
- Killworth, P.D. and McDonald, N.R. (1993). Maximal reduced-gravity flux in rotating hydraulics. *Geophys. Astrophys. Fluid Dynam.*, **70**, 31–40.
- Kinder, T.H., Chapman, D.C. and Whitehead, J.A. (1986). Westward intensification of the mean circulation on the Bering Sea Shelf. *J. Phys. Oceanogr.*, **16**, 1217–1229.

- Nof, D. (1986). Geostrophic shock waves. *J. Phys. Oceanogr.*, **16**, 886–901.
- Nof, D. (1988). Out flows dynamics. *Geophys. Astrophys. Fluid Dynam.*, **40**, 165–193.
- Nof, D. (1990). Why are some boundary currents blocked by the Equator? *Deep-Sea Res.*, **37**, 853–873.
- Nof, D. (1995). Choked flows and wind-driven interbasin exchange. *J. Mar. Res.*, **53**, 23–48.
- Nof, D. and Olson, D. (1983). On the flow through broad gaps with application to the Windward Passage. *J. Phys. Oceanogr.*, **13**, 1940–1956.
- Pratt, L.J. (1983). On inertial flow over topography. Part 1. Semigeostrophic adjustment to an obstacle. *J. Fluid Mech.*, **131**, 195–218.
- Pratt, L.J. (1984). On inertial flow over topography. Part 2. Rotating channel flow near the critical speed. *J. Fluid Mech.*, **145**, 95–110.
- Pratt, L.J. (1986). Hydraulic control of sill flow with bottom friction. *J. Phys. Oceanogr.*, **16**, 1970–1980.
- Pratt, L.J. (1987). Rotating Shocks in a Separated Laboratory Channel Flow. *J. Phys. Oceanogr.*, **17**, 483–491.
- Pratt, L.J. (1997a). Hydraulically drained flows in Rotating Basins Part I: Method. *J. Phys. Oceanogr.*, **27**, 2509–2521.
- Pratt, L.J. (1997b). Hydraulically drained flows in Rotating Basins Part II: Steady Flows. *J. Phys. Oceanogr.*, **27**, 2522–2535.
- Pratt, L.J. and Armi, L. (1987). Hydraulic control of flows with nonuniform potential vorticity. *J. Phys. Oceanogr.*, **17**, 2016–2029.
- Pratt, L.J. and Lundberg, P.A. (1991). Hydraulics of rotating strait and sill flow. *Ann. Rev. Fluid Mech.*, **23**, 81–106.
- Pratt L.J. and Chechelnitsky, M. (1997). Principles for capturing the upstream effects of deep sills in low-resolution ocean models. *Dyn. Atmos. Oc.*, **26**, 1–25.
- Rudnick, D. (1997). Direct Velocity Measurements in the Samoan Passage. *J. Geophys. Res.*, **102**, 3293–3302.
- Rydberg, L. (1980). Rotating hydraulics on deep-water channel flow. *Tellus*, **32**, 77–89.
- Saunders, P.M. (1987). Flow through Discovery Gap. *J. Phys. Oceanogr.*, **17**, 631–643.
- Saunders, P.M. (1990). Cold outflow from the Faeroe Bank Channel. *J. Phys. Oceanogr.*, **20**, 29–43.
- Saunders, P.M. (1994). The flux of overflow water through the Charlie–Gibbs Fracture Zone. *J. Geophys. Res.*, **99**, 12343–12355.
- Shen, C.Y. (1982). The rotating hydraulics of open-channel flow between two basins. *J. Fluid Mech.*, **112**, 161–188.
- Smith, P.C. (1976). Baroclinic Instability in the Denmark Strait Overflow. *J. Phys. Oc.*, **6**, 355–371.
- Speer, K.G. and Zenk, W. (1993). The flow of Antarctic Bottom Water into the Brazil Basin. *J. Phys. Oc.*, **23**, 2667–2682.
- Spitz, Y.H. and Nof, D. (1991). Separation of boundary currents due to bottom topography. *Deep-Sea Res.*, **38**, 1–20.
- Stern, M.E. (1974). Comment on rotating hydraulics. *Geophys. Fluid Dyn.*, **6**, 127–130.
- Stern, M.E. (1980). Geostrophic fronts, bores, breaking and blocking waves. *J. Fluid Mech.*, **99**, 687–704.
- Stern, M.E., Whitehead, J.A. and Hua, B.-L. (1982). The intrusion of a density current along the coast of a rotating fluid. *J. Fluid Mech.*, **123**, 237–265.
- Whitehead, J.A. (1985). The deflection of a baroclinic jet by a wall in a rotating fluid. *J. Fluid Mech.*, **157**, 79–93.
- Whitehead, J.A. (1986). Flow of a homogeneous rotating fluid through straits. *Geophys. Astrophys. Fluid Dynam.*, **36**, 187–205.
- Whitehead, J.A. (1989). Internal hydraulic control in rotating fluids – applications to oceans. *Geophys. Astrophys. Fluid Dynam.*, **48**, 169–192.

- Whitehead, J.A. (1998). Topographic control of ocean flows in deep passages and straits. *Reviews of Geophys.*, **36**, 423–440.
- Whitehead, J.A. and Porter, D.L. (1977). Axisymmetric critical withdrawal of a rotating fluid. *Dyn. Oc. Atmos.*, **2**, 1–18.
- Whitehead, J.A., Jr. and Worthington, L.V. (1982). The flux and mixing rates of Antarctic Bottom Water within the North Atlantic. *J. Geophys. Res.*, **87**(C10), 7903–7924.
- Whitehead, J.A., Leetmaa, A. and Knox, R.A. (1974). Rotating hydraulics of strait and sill flows. *Geophys. Fluid Dynam.*, **6**, 101–125.
- Woods, A.W. (1993). The topographic control of planetary-scale flow. *J. Fluid Mech.*, **247**, 603–621.